Enhanced glycolysis-derived lactate promotes microglial activation in Parkinson's disease via histone lactylation

Qixiong Qin

  Huazhong University of Science and Technology

Danlei Wang

  Huazhong University of Science and Technology

Yi Qu

  Huazhong University of Science and Technology

Jiangting Li

  Huazhong University of Science and Technology

Ke An

  Huazhong University of Science and Technology

Zhijuan Mao

  Huazhong University of Science and Technology

Jingyi Li

  Huazhong University of Science and Technology

Yongjie Xiong

  Huazhong University of Science and Technology

Zhe Min

  Huazhong University of Science and Technology

Zheng Xue (✉ xuezheng@hust.edu.cn)

  Huazhong University of Science and Technology

Research Article

Abstract

The metabolic switch from oxidative phosphorylation to glycolysis is a vital hallmark and prerequisite for microglia phenotype transition. Recently, histone lactylation was shown to promote macrophage homeostatic gene expression via transcriptional regulation. However, the role of histone lactylation in regulating microglia function in Parkinson's disease (PD) remains unclear. Here, we show that glycolytic inhibitor 2-deoxy-D-glucose alleviatesmicrogliosis, neuroinflammation, and dopaminergic neuronal damage by reducing lactate accumulation. Notably, histone lactylation, especially H3K9la, is markedly increased in microglia within the substantia nigra of a mouse model of PD and lipopolysaccharide-stimulated primary microglia. Mechanistically, enhanced glycolysis-derived lactate induces H3K9la enrichment at the promoter of solute carrier family 7 member 11 (Slc7a11), promoting its transcription. Inhibition ofSLC7A11 by sulfasalazine mitigates microglia-mediated neuroinflammation and improves motor function in the mouse model PD mice. Moreover, lactate-induced histone lactylation is dependent on the p300/CBP. Collectively, ourfindings demonstrate that augmented glycolysis-derived lactate promotes microglial activation via histone lactylation and provide a novel therapeutic strategy for PD.

1. Introduction

Parkinson's disease (PD) is the second most common neurodegenerative disease characterized by progressive loss of dopaminergic (DA) neurons and classical motor features of parkinsonism associated with Lewy bodies.[1, 2] Nneuroinflammation induced by excessive microgliosis and proinflammatory activation plays a critical role in DA neuronal damage and PD progression.[3, 4] Microglia, as critical innate immune cells, play a key role in brain immune surveillance and maintaining brain homeostasis. However, upon inflammatory stimulation, microglia become activated and release large amounts of proinflammatory cytokines, creating an inflammatory microenvironment and leading to neuronal damage.[5] Therefore, inhibiting microglia-mediated neuroinflammation may ameliorate PD progression.

Although the underlying mechanisms of microglial activation remain unclear, evidence suggests that metabolic reprogramming provides new insights into inflammation.[6, 7] That is, microglia undergo a metabolic switch from oxidative phosphorylation (OXPHOS) to aerobic glycolysis in response to inflammatory factors, such as lipopolysaccharide (LPS), α-synuclein preformed fibril (PFF) or amyloid-beta plaque (Aβ).[8, 9] Further studies demonstrated that lactate, the end product of glycolysis, acts as an important signaling molecule to regulate the function of microglia.[10, 11] In particular, we previously reported that inhibition of glycolysis and lactate accumulation attenuates DA neuronal apoptosis and microgliosis in a mouse model of PD.[12] Thus, reprogramming microglial glycolysis may be a promising strategy to mitigate the inflammatory activation of microglia and ameliorate neuroinflammation and PD progression.

Recently, post-translational modifications (PTMs) mediated by metabolites have been recognized as a key mechanism in the metabolic regulation of immune responses[13]. Notably, Zhang *et al.*[13] discovered

that lactate can serve as a substrate to induce histone lactylation by generating lactyl-CoA and adding a lactyl group to the histone lysine (K) residue.[14] Subsequent studies found that histone lactylation contributes to macrophage M1/2 polarization, tumor development, and neural excitation.[15−17] However, the role of histone lactylation in the activation of microglia remains largely unexplored.

Accordingly, we hypothesize that histone lactylation induced by glycolysis-derived lactate may contribute to microglial activation in PD. To test this hypothesis, we investigated the role of glycolysis and histone lactylation in microglial activation in a murine PD model. Our findings indicate that enhanced glycolysis-derived lactate promotes the pro-inflammatory activation of microglia through histone lactylation in PD, especially H3K9la. By performing cleavage under targets and tagmentation (CUT&Tag) and RNA-seq, we found that H3K9la is enriched at the *Slc7a11* promoter and induces its transcription. Importantly, we demonstrate that inhibition of SLC7A11 attenuates microglia-mediated neuroinflammation and improves motor function in PD mice. Collectively, our study provides new insights into the interaction between metabolic reprogramming and epigenetics in PD microglial activation.

2. Results

2.1 Inhibition of glycolysis alleviates microglial activation and DA neuronal damage and improves motor function in PD mice

To explore the role of glycolysis in PD pathology, we used 2-DG to inhibite glycolysis in MPTP-induced murine model of PD. The substantia nigra (SN) of MPTP-treated mice had elevated lactate (Fig. 1A), *Hk2* mRNA (Fig. 1B), and HK2 and LDHA protein levels compared to control mice (Figure S1F, G, Supporting Information). However, 2-DG treatment significantly suppressed the upregulation of lactate, HK2 and LDHA.

To assess the effect of glycolysis inhibition on the motor functions of MPTP-treated mice, we conducted the rotarod test, pole test, and OFT. MPTP induced motor dysfunction in mice, as evidenced by shorter residence time on the rotarod (Figure S1A, Supporting Information), longer time on the pole (Figure S1B), shorter movement distance, and longer immobility time in OFT (Figure S1C, D, Supporting Information). In contrast, 2-DG treatment reversed motor dysfunction in MPTP-treated mice (Figure S1A−D, Supporting Information). These results suggest that glycolysis inhibition improves motor dysfunction in MPTP-induced murine model of PD.

Next, we investigated the impact of glycolysis inhibition on microglial activation and DA neuronal damage. The TH protein abundance that decreased in MPTP-treated mice was reversed by 2-DG (Fig. 1C, D). Moreover, immunostaining revealed an increased number of microglia and a decreased number of DA neurons in MPTP mice compared to control mice, which were reversed by 2-DG treatment (Figure S1H−J, Supporting Information).

2.2 Inhibition of glycolysis alleviates microglial activation and DA neuronal damage by reducing lactate accumulation

Typically, activated microglia are categorized as either M1 (neurotoxic) or M2 (neuroprotective).[18] To explore whether glycolysis inhibition affects microglial phenotypes, we performed co-immunostaining of IBA1 with M1 marker (CD86 and CD68) and observed an increased immunoreactivity of CD86 (Fig. 1E, F) and CD68 (Figure S1K, L, Supporting Information) in the SN of MPTP mice. However, this effect was reduced by 2-DG treatment. Furthermore, 2-DG treatment decreased the levels of TNF-α and increasedthe expression of ARG1 in MPTP-treated mice (Fig. 1C, D, Figure S1E, Supporting Information). These findings indicate that inhibiting glycolysis alleviates the proinflammatory activation of microglia and DA neuronal damage in the mouse model of PD.

To further confirm the protective effect of glycolysis inhibition, we established an inflammatory PD mouse model by injecting LPS into the SN. As expected, a decreased number of TH⁺ cells and an increased number of IBA⁺ microglia were observed in LPS-injected mice, which was reversed following 2-DG treatment (Fig. 1I−K). This result was supported by western blotting, which showed an increased abundance of TH⁺ cells in the SN of LPS-treated mice following 2-DG injection (Fig. 2G−H). Moreover, immunofluorescence staining showed decreased immunoreactivity of the M1 marker CD68 (Figure S1M, N, Supporting Information) and increased immunoreactivity of the M2 marker CD206 (Fig. 2L-M) in LPS-injected mice. These data indicate that inhibition of glycolysis promotes microglia to switch toward the M2 neuroprotective phenotype and alleviate DA neuronal damage in LPS-induced mouse model of PD.

In agreement with the results in MPTP and LPS-treated mice, we observed that mRNA expressions of *Glut1*, *Hk2*, *Ldha* were upregulated (Fig. 2A) and lactate concentrations were increased (Fig. 2B) in LPS-stimulated primary microglia. To elucidate the causal link between glycolysis inhibition and microglia activation, we examined changes in the morphology and phenotype of primary microglia stimulated by LPS and treated with 2-DG. 2-DG treatment downregulated *Il1b*, *Tnf*, *Il6*, and *Nos2* mRNA expression (Fig. 2E) and upregulated *Cd206* and *Ym1* expression (Fig. 2C, D), which was confirmed by western blotting (Figure S2A, B, Supporting Information). Moreover, treatment with 2-DG suppressed the ameboid morphology of primary microglia stimulated by LPS (Figure S2C, Supporting Information). Our data indicates that enhanced glycolysis was necessary for microglial activation.

It has shown that lactate is an essential signaling molecule in cellular biological processes.[10] To explore the global effects of lactate in microglial activation, we pretreated LPS-stimulated primary microglia with sodium oxalate and observed reduced production of lactate (Fig. 2H) and decreased LDHA levels (Fig. 2F, G). Moreover, sodium oxalate treatment decreased iNOS protein level (Fig. 2F, G) and *Il1b*, *Tnf*, and *Il6* mRNA expression (Fig. 2I−K) in LPS-stimulated primary microglia. To assess the potential effect of lactate on the pro-inflammatory activation of microglia cells, we stimulated primary microglia with soluble lactate. The mRNA expressions of *Il1b*, *Tnf*, and *Il6* was up-regulated in a lactate concentration-

dependent manner (Fig. 2L). These findings suggest that enhanced glycolysis-derived lactate is a key contributor to microglia activation.

2.3 Enhanced glycolysis-derived lactate promotes microglial activation through histone lactylation

Lactate induces lactylation via the addition of a lactyl group to histone lysine (K) residues, thus regulating gene transcription in macrophages.[14] To determine whether histone lactylation is involved in microglia activation, we stimulated primary microglia with LPS, IL-4, and exogenous lactate, and quantified pan-Kla and H3K9la levels. As shown in Fig. 3A, LPS stimulation significantly increased the levels of pan-Kla, while IL-4 stimulation did not. Moreover, exogenous lactate increased pan-Kla levels in a concentration-dependent manner, particularly at the 17 KD position (histone) (Fig. 3B). We then detected the sites of histone lactylation by western blotting and observed a significant increase in H3K9la levels after LPS stimulation, which was reduced by 2-DG treatment (Fig. 3C, D).

Histone lactylation is increased in the brains of 5XFAD model mice and contributes to microglial dysfunction.[19] Here, we observed an increase in the levels of pan-Kla and H3K9la in the SN of MPTP-treated mice (Fig. 3E, F and Figure S3A, B, Supporting Information). To determine the cellular localization of H3K9la, co-immunostaining was performed with H3K9la and different cell markers. We found that H3K9la was widely expressed in all cells (Fig. 3G, H, Figure S3C–H, Supporting Information). Compared with the control group, the fluorescence intensity of H3K9la in microglia was increased in MPTP-treated mice (Fig. 3G, H), whereas no significant difference was observed in other cells (Figure S3C–H, Supporting Information). These results indicate that histone lactylation is increased in microglia in the SN of the mice model of PD.

Next, we verified the levels of glycolysis and lactylation in A53T mice. The abundance of HK2 and LDHA protein, and lactate concentration were increased in the microglia within the SN of A53T mice compared to wild-type (WT) mice (Figure S3I–K). Moreover, the levels of LDHA expression in microglia were elevated in A53T mice (Figure S3L–M). Additionally, pan-Kla and H3K9la levels were increased in the SN of A53T mice (Fig. 3I, J). Consistent with the findings in MPTP mice, we found a significant increase in the intensity of H3K9la fluorescence in the microglia within the SN of A53T mice (Fig. 3K, L). These data indicate that glycolysis and histone lactylation are increased in the microglia within the SN of A53T mice.

2.4 Inhibition of glycolysis decreases microglia activation by reducing histone lactylation

To determine whether inhibiting glycolysis can alleviate microglial activation by reducing histone lactylation, we treated LPS-stimulated primary microglia with 2-DG. Results showed a reduction in pan-Kla and H3K9la levels (Figure S4A, B, Supporting Information). Similarly, inhibiting the production of lactate with sodium oxalate (Fig. 4A–C) or *Ldha*-siRNA (Fig. 4A, B, Figure S4 C, D, Supporting

Information) also significantly reduced pan-Kla and H3K9la levels in LPS-stimulated primary microglia. Moreover, we found that the increased fluorescence intensity of pan-Kla (Figure S4E, F, Supporting Information) and H3K9la (Fig. 4C, D) in the microglia of MPTP mice was reversed by 2-DG treatment. These results were verified in LPS-induced PD mice (Fig. 4E, F, Figure S4G, H, Supporting Information). And western blotting showed that 2-DG treatment reduced the levels of pan-Kla and H3K9la in the SN of LPS-injected mice (Fig. 4G−I). Moreover, as showed in Fig. 2F-K, sodium oxalate treatment decreased iNOS protein level and Il1b, Tnf, and Il6 mRNA expression in LPS-stimulated primary microglia. Therefore, these data suggest that inhibiting glycolysis may alleviate microglial activation by reducing histone lactylation.

2.5. H3K9la promotes the activation of microglia by activating SLC7A11 gene transcription

To screen the potential targets of H3K9la, we performed CUT&Tag and RNA-seq analyses (Figure S5A, Supporting Information). Volcano plots of the differentially expressed gene (DEG) analysis showed that solute carrier family 7 member 11 (*Slc7a11*) was upregulated in LPS-stimulated primary microglia (Fig. 5A). The peak map of the identified candidate genomic loci indicated that H3K9la was enriched at the *Slc7a11* promoter (Fig. 5B). Chip-qPCR confirmed the enrichment of H3K9la in the promoter of *Slc7a11* in LPS-stimulated primary microglia which was decreased by 2-DG and soluble oxalate treatment (Fig. 5C). Notably, the *Slc7a11* mRNA expression was significantly upregulated in LPS-stimulated primary microglia (Fig. 5D). These data indicate that H3K9la promotes the transcription of *Slc7a11* in microglia.

We then explored the role of SLC7A11 in microglial activation. Treatment of LPS-stimulated primary microglia with an SLC7A11 inhibitor, erastin, significantly reduced the expression of *Il1b, Nos2, Il6,* and *Tnf* mRNA (Fig. 5E). These results were further confirmed by western blotting and immunostaining (Fig. 5F, G, Figure S5B, C, Supporting Information). Inverted fluorescence microscopy revealed that erastin inhibited the activation of primary microglia (Figure S5D, Supporting Information). Moreover, *Slc7a11* knockout significantly deregulated the expression of *Il1b, Il6, Nlrp3, Cd86* and *Cd80* mRNA (Figure S5E, Supporting Information). Next, we performed CCK8 assays to assess the impact of MCM on SH-SY5Y cell apoptosis (Figure S5F, Supporting Information). Erastin treatment alleviated MCM-induced apoptosis in SH-SY5Y cells (Fig. 5H). Collectively, these results suggest that inhibition of SLC7A11 alleviates microglial activation and MCM-mediated SH-SY5Y cell apoptosis.

SAS is an azo-bridged anti-inflammatory agent commonly used to treated chronic inflammatory diseases that was recently identified as a potent inhibitor of SLC7A11.[20] Therefore, to explore the effect of SLC7A11 on motor function, we intraperitoneally injected LPS-induced PD mice with SAS (Fig. 6A, Figure S6A, B, Supporting Information). Injection of the SN with LPS induced motor dysfunction in mice, as evidenced by shorter residence time on the rotarod (Fig. 6B), longer time on the climbing pole (Fig. 6C), as well as shorter movement distance, mean speed and longer immobility time in the open field (Fig. 6D−G).

In contrast, SAS administration reversed the motor dysfunction of LPS mice (Fig. 6B–G). These results indicate that inhibition of SLC7A11 improves motor dysfunction in LPS-induced PD mice.

We then investigated the effect of SLC7A11 on microglial activation and DA neuronal damage. SAS treatment increased the number of TH$^+$ cells, while concomitantly decreasing the number of IBA1$^+$ cells in LPS-induced PD mice (Fig. 6H–J). Moreover, SAS administration reduced the immunoreactivity of CD86 (M1 marker) in LPS-induced PD mice (Fig. 6K, L). We also found that the mRNA expression of *Il1b*, *Cd86*, *Nlrp3*, and *Cd80* was downregulated in the SN of LPS mice following SAS treatment (Fig. 6M). Taken together, our results indicate that inhibiting SLC7A11 mitigates DA neuronal injury by reducing microglial activation and expression of pro-inflammatory cytokines.

2.7 p300/CBP mediates lactate-induced histone lactylation and microglial activation

Acetyltransferases p300 and its homolog CREB-binding protein C (CBP) transfer L-lactyl-CoA onto histones to induce lactylation.[14, 21] Herein, we observed increased levels of p300 and CBP in LPS-stimulated primary microglia (Figure S7A, B, Supporting Information). Therefore, to determine whether p300 and CBP mediated histone lactylation and microglial activation, we inhibited p300/CBP with C646 and found that the levels of pan-Kla and H3K9la were diminished (Fig. 7A, B). Meanwhile, the expression of TNF-α, iNOS2, and NLRP3 proteins was also markedly suppressed (Figure S7C, D, Supporting Information). To exclude the additional effect of C646, we knocked down *p300* and *Cbp* using siRNA (Fig. 7C, D). Results show that *p300* knockdown reduced the expression of *Il6* and *Nos* mRNA, while upregulating that of *Arg1* (Fig. 7E). In addition, the increased levels of pan-Kla and H3K9la in LPS-stimulated primary microglia were reduced following *p300* knockdown (Fig. 7F, G). Similarly, we found that *Cbp* knockdown not only down-regulated the expression of *Il6*, *Il1b*, and *Nos2* (Figure S7E, Supporting Information) but also reduced pan-Kla and H3K9la levels (Fig. 7H, I). These results reveal that lactate-induced histone lactylation and proinflammatory factors expression depends on p300/CBP.

3. Discussion

Microglia-mediated neuroinflammation plays a key role in the pathogenesis of PD.[8, 22] Therefore, elucidating the mechanisms underlying microglial activation may provide potential therapeutic target to reduce microglia-mediated neuroinflammation and facilitate the development of effective therapeutic strategies against neurodegenerative diseases. In the present study, we demonstrated that inhibiting glycolysis with 2-DG alleviated microglial activation and DA neuronal damage, while improving motor dysfunction in PD mice. Moreover, histone lactylation, in particular, H3K9la was increased in activated microglia within the SN of the mouse model of PD. H3K9la activated the transcription of *Slc7a11* and promoted pro-inflammatory activation of microglia. Importantly, inhibition of SLC7A11 suppressed microglia activation and improved motor function in the mice. Additionally, we showed that the lactate-induced histone lactylation is depended on p300/CBP. Taken together, our findings reveal that enhanced

glycolysis contributes to microglial activation-mediated neuroinflammation via the H3K9la/SLC7A11 pathway, which may provide a new perspective for immune-metabolism therapy of PD.

We started our study by observing that inhibition of glycolysis enzymes blocked LPS-induced microglial activation and pro-inflammatory cytokine expression. This highlighted the critical role of glycolysis in the inflammatory activation of microglia. Indeed, inhibition of glycolysis has been shown to exert neuroprotective effects by suppressing pro-inflammatory activation of microglia and neuroinflammation in stroke and perioperative neurocognitive disorders.[24-26] Moreover, our previous study reported that glycolysis inhibition mitigates apoptosis of DA neurons by reducing lactate accumulation in MPTP-treated mice.[12] Here, we confirmed that inhibiting glycolysis alleviated microglial activation and reversed motor dysfunction in a mice model of PD. Our findings demonstrate that inhibition of microglial glycolysis attenuates neuroinflammation and neuronal damage mediated by microglial activation.

Although it is widely known that metabolic reprogramming is involved in microglia activation, the specific underlying mechanisms remain unclear. Lactate, previously considered a waste product of aerobic glycolysis, serves as a potent signaling molecule that regulates cellular functions in immune cells.[27, 28] In the tumor microenvironment, lactate promotes the M2 polarization of tumor-associated macrophages and facilitates the immune escape of tumor cells. However, a recent study indicated that lactate exacerbates inflammation by increasing IL-17 production via the PKM2/STAT3/RORγt pathway in chronic inflammatory diseases.[29] Moreover, targeting *Ldha* has been shown to reduce macrophage migration and inflammatory cytokine release in multiple sclerosis.[30] Therefore, the response of immune cells to lactate varies in different disease states. Here, we demonstrated that exogenous lactate promoted the expression of proinflammatory cytokines, an effect that was prevented by reducing lactate production with sodium oxalate. Given the significant increase in the CSF lactate concentration of patients with PD,[31] we propose that lactate derived from enhanced glycolysis may be a key contributor to microglial activation.

Recently, Zhang *et al*. identified a novel PTM, namely, histone lysine lactylation, that uses lactate as its main substrate and drives transcription of reparative genes in the late stage of macrophage M1 polarization.[14] Hence, lactylation connects immune cell metabolism and gene regulation, which has opened a new door for the research of immunometabolism.[14] Notably, histone lactylation occurs widely throughout the CNS and is involved in the regulation of neuronal differentiation and neural excitation.[17, 32] Intriguingly, a recent study reported that H4K12la was elevated in microglia adjacent to Aβ plaques in 5XFAD model mice. Meanwhile, AD patients exhibited increased *PKM2* transcription, forming a glycolysis/H4K12la/PKM2 positive feedback loop, which exacerbated microglial dysfunction.[19] However, the role of histone lactylation in PD has not been reported. For the first time, we demonstrated that histone lactylation (H3K9la) was increased in the SN of PD mice, particularly in activated microglia. Meanwhile, glycolysis inhibition reduced H3K9la and microglia M1 polarization, while improving motor function in PD mice. These findings highlight the critical role of histone lactylation in microglia-mediated neuroinflammation in neurodegenerative diseases.

To further explore the potential role of H3K9la in microglia activation, we performed CUT&Tag and RNA-seq analysis and identified *Slc7a11* as the target gene of H3K9la. SLC7A11 is a subunit of cystine-glutamate antiporter that exchanges cysteine for glutamate and promotes glutathione synthesis and oxidative protection.[33] Previous studies have reported that SLC7A11 is widely expressed in the CNS and is associated with microglial activation.[34] Moreover, inhibition of SLC7A11 by SAS reduces microglial activation, exerting neuroprotective effects in ischemic stroke, amyotrophic lateral sclerosis, and spinal cord injury.[20, 35, 36] Consistent with these findings, we demonstrated that SAS reduced microglial activation and neuroinflammation and improved motor function in LPS-induced PD mice. Given glycolysis inhibition deregulated H3K9la enrichment at the *Slc7a11* promoter and *Slc7a11* expression, we proposed that histone lactylation activated microglia by promoting *Slc7a11* transcription. However, it should be noted that SLC7A11 is also a hallmark of ferroptosis, the harmful effects of which have been widely reported in neurons. However, the role of ferroptosis in microglia activation remains controversial.[37, 38] Interestingly, a recent study revealed that M1-polarized microglia are resistant to ferroptosis.[39, 40] Moreover, promoting ferroptosis in M1 microglia can reduce neuroinflammation and mitigate brain injury following subarachnoid hemorrhage.[41] Nonetheless, further research is needed to determine whether SLC7A11 promotes microglial activation through ferroptosis.

Changes in PTMs over time and space are important biological events that regulate protein function.[42, 43] Recently, p300, a key acetyltransferase was found to transform lactate into L-lactyl-CoA and transfer it onto histones to induce histone lactylation.[14, 21] In this study, we observed that lactate-induced H3K9la and pro-inflammatory gene expression were dependent on p300/CBP in microglia, as evidenced by their diminished concentrations following p300/Cbp knockdown. Our findings were supported by studies revealing that p300/CBP promotes HMGB1 lactylation in polymicrobial sepsis[21] and the lactylation of profibrotic genes in lung myofibroblasts.[43] However, we do not consider it an ideal target for modulating lactylation, as targeting p300 may simultaneously impact lactylation and acetylation. Therefore, it is necessary to identify the specific lactyl-transferase responsible for lactylation.

This study is limited in that we inhibited glycolysis by intraperitoneal injection of 2-DG, which may have additional effects beyond the inhibition of lactate production. Future studies using microglial *Ldha* knockout mice may help elucidate the role of lactate in microglial activation. In addition, we cannot efficiently generate site mutations in histone H3 to evaluate the specific effect of H3K9la in microglia, which weakens the persuasiveness of the experiment. Furthermore, although the temporal and spatial dynamics of activating gene transcription via histone lactylation differs from histone acetylation, the interaction or competition between the two requires further exploration. Finally, we showed that pharmacological inhibition of SLC7A11 alleviated microglia activation and neuroinflammation in a mouse model of PD. However, whether this process is related to ferroptosis must be further confirmed.

4. Conclusion

In conclusion, our findings demonstrate that enhanced glycolysis induces pro-inflammatory activation of microglia via the histone lactylation/SLC7A11 pathway as a key event in PD pathogenesis, suggesting that microglial metabolic immune functions may be a potential target for PD therapy.

5. Experimental Section

Animals and Ethics

Male C57BL/6J mice (7−8 weeks old, 22−25 g) were procured from Nanjing Gempharmatech Co. Ltd. A53T transgenic (A53T) mice were obtained from Beijing HuAFukang Biotechnology Co., Ltd. The mice were housed in a specific pathogen-free animal facility under standard conditions, maintained at 21−25°C with a 12-h light/dark cycle, and free access to food and water. A53T mice began to exhibit behavioral abnormalities and arched back at 8−9 months, and most mice had obvious movement disorders at 14−15 months. In this study, male A53T mice aged 10−12 months with onset disease were used for follow-up experiments, and C57BL/6J mice matched by age and sex were used as WT controls. All animal procedures were approved by the institutional animal care and use committee of Tongji Hospital.

Establishment of the PD mouse model and drug treatment

A subacute PD mouse model was established using 1-methyl-4-phenyl-1,2,3,6-tetrahydropyridine (MPTP). Twenty-five mice were divided randomly into three groups: control group (PBS), model group (MPTP), and positive drug group (2-DG+MPTP). Mice in the MPTP group and 2-DG+MPTP group were intraperitoneally injected with MPTP (MPTP, 30 mg/kg, Sigma) once daily for five consecutive days, while mice in the PBS group received a similar volume of PBS injected intraperitoneally. For 2-DG treatment, mice in the 2-DG+MPTP group were intraperitoneally injected with 2-DG (250 mg/kg) 3 days before receiving the MPTP injection; 2-DG was administered 2 h before the MPTP injection. Mice in the PBS group and MPTP group received a similar volume of PBS injected intraperitoneally.

An inflammatory PD mouse model was established by injecting LPS into the SN. Briefly, 30 mice were divided randomly into three groups: control group (PBS), model group (LPS), and positive drug group (2-DG+LPS). For the LPS group and 2-DG+LPS group, 2.5 μg of LPS was injected into the right SN using a stereotaxic apparatus, while mice in the PBS group received a similar volume of PBS. For 2-DG treatment, mice in the 2-DG+LPS group were intraperitoneally injected with 2-DG (250 mg/kg) 3 days before the LPS injection and continued for 5 days after the LPS injection. Mice in the PBS group and MPTP group received a similar volume of PBS by intraperitoneal injection.

To explore the effect of the SLC7A11 inhibitor sulfasalazine (SAS) on microglial activation, 32 mice were divided randomly into four groups: control group (PBS), model group (LPS), drug group (SAS), and drug+model group (SAS+LPS). We first established an inflammatory PD mouse model. For SAS treatment, 150 mg/kg of SAS was administered intraperitoneally twice daily before LPS stereotaxic injection and continued for 7 days after LPS injection. Mice in the PBS group and LPS group received a similar volume of PBS injected intraperitoneally.

Behavioral test

Behavioral tests were performed on day 7 after the last MPTP administration and LPS injection.

Rotarod test: The Rotarod Treadmill (IITC) was used after a three-day training period. In the formal test, mice were placed on the rotarod instrument, set to uniformly accelerate from 5 to 45 rpm over 5 min. Each mouse underwent three trials with at least 30 min between tests, and the results were averaged. The time that mice stayed on the rotating axis before falling was recorded.

Pole test: A vertical wooden pole 50 cm long and 1 cm in diameter, with a cork at the top was employed. Before the formal test, the mice were trained for two consecutive days; each training session comprised three test trials. In the formal test, mice were placed on the cork, and the time it took to climb from the cork to the bottom of the pole was recorded.

Open-field test (OFT): Mice were placed and allowed to explore freely in an open-field reaction box (30 cm in length, 30 cm in width, and 35 cm in height) for 5 min. The ANY-MAZE video tracking system (Version 7.16, Stoelting, USA) was used to record their movement distance and immobility time.

Preparation of brain samples

After behavioral testing, mice were euthanized using 5% isoflurane to induce deep anesthesia. For immunofluorescence analysis, mice underwent cardiac perfusion with 30 mL of pre-cooled 1% phosphate-buffered saline (PBS) followed by 30 mL of pre-cooled 4% paraformaldehyde (PFA). After perfusion, the brain was removed, post-fixed in 4% PFA at 4 °C for 12 h, and then completely dehydrated in 30% sucrose. Serial 20 μm coronal sections were cut by a constant temperature (-23 °C) frozen slicer. For qPCR and western blot analysis, mice were perfused with 30 mL of pre-cooled 1% PBS. Their brains were extracted, rapidly frozen in liquid nitrogen-cooled isopentane, and stored at -80 °C.

Measurement of lactate concentration

Lactate concentrations in the cell culture medium were determined using a Lactate Assay Kit (A019-2-1, Jiancheng Bioengineering Institute, Nanjing, China) following the manufacturer's recommendations. Lactate concentrations in the SN and striatum were measured using the L-Lactate Assay Kit (Colorimetric/Fluorometric, ab65330, Abcam) according to the manufacturer's protocol.

Immunofluorescence staining

Brain slides were permeabilized with 0.25% Triton X-100 and blocked with QuickBlock™ Blocking Buffer (Beyotime, Nanjing, China) for 15 min. Brain sections were then incubated with primary antibodies for 12 h at 4 °C: rabbit anti-tyrosine hydroxylase (TH) (1:500; Abcam), sheep anti-TH (1:500; Novus), goat anti-IBA1 (1:500; Abcam), rat anti-CD68 (1:500; Bio-Rad), rat anti-CD86 (1:500; Abcam), rabbit-Mannose Receptor 1 (MRC1/CD206), rabbit anti-Lactate dehydrogenase A (LDHA) antibody (1:200, Cell Signaling Technology, CST), mouse anti-GFAP (1:200, CST), mouse anti-NeuN antibody (1:100, Proteintech), rabbit

anti-pan histone lysine lactylation (pan-Kla) (1:100; PTM BIO), rabbit anti-H3K9la (1:100; PTM BIO), and rabbit anti-SLC7A11 antibody (1:100, Proteintech). Subsequently, slides were incubated with Alexa Fluor 488 or Alexa Fluor 594 (Yeasen Biotechnology) in the dark at room temperature for 1 h, and then stained with 4,6-diamidino-2-phenylindole. Images were captured using fluorescence and confocal microscopy (Olympus FV1200, Japan) and analyzed using ImageJ software (Java 1.8.0, National Institutes of Health, USA).

Culture and stimulation of primary microglia

Primary microglia were isolated from neonatal (P0–P3) C57BL/6J mice. Briefly, the brain tissue was digested with 0.125% trypsin for 15 min at 37 °C. The cells were resuspended in DMEM/F12 medium containing 20% fetal bovine serum and cultured in a 5% CO_2 incubator at 37 °C. After 36 h, the medium was replaced with high-glucose DMEM containing 20% fetal bovine serum. After 10–12 days of culture, microglia were isolated from the mixed glial cultures.

Primary microglia were stimulated with 0.2 μg/mL LPS (0111: B4, Sigma-Aldrich, St. Louis, MO, USA) for 24 h. In some experiments, microglia were pretreated with 2-DG (0.5, 1, and 2 μM) to inhibit glycolysis, sodium oxalate (10 μM) to reduce the production of lactate, C646 (5 μM) to inhibit p300/CBP, or erastin (20 μM) to block SLC7A11 before addition of LPS. siRNA was used to knock down p300, *Cbp, Ldha*, and *Slc7a11*, and transfection was performed using Lipofectamine 3000. The cells were collected for subsequent experiments.

Primary microglia-conditioned medium (MCM) treatment SH-SY5Y cells

Briefly, primary microglia were treated with 20 μM erastin for 30 min and then with 0.2 μg/mL LPS for 4 h, followed by medium replacement. After 24 h, the medium was collected and mixed with fresh medium in a 1:1 ratio to obtain an MCM (Figure S5F). The MCM was used to stimulate human neuroblastoma SH-SY5Y cells, and the activity of cells was evaluated by CCK8 assay.

Cell viability assay

Cell viability was assessed using the CCK-8 kit (Yeasen, Shanghai, China). Briefly, 100 μL of medium containing 10 μL of CCK-8 reagent was added to each well and incubated at 37 °C for 4 h. Absorbance was measured at 450 nm using a microplate reader (Thermo Fisher Scientific).

Western blot analysis

Primary microglia and brain tissue were lysed in RIPA buffer with PMSF, phosphatase inhibitor, and a protease inhibitor cocktail (Servicebio, Wuhan, China). Protein concentrations were measured using a bicinchoninic acid assay kit (Beyotime, Shanghai, China). Equal amounts of protein extracts (20–40 μg) were separated by 8–15% SDS-PAGE and transferred onto 0.22 μm nitrocellulose membranes. The membranes were blocked with Quick Block western blocking buffer and incubated with primary antibodies for 12 h at 4 °C and subsequently with secondary antibodies (Servicebio, Wuhan, China) for 1

h at room temperature. Images were acquired using an imaging system (GelView 6000 Pro, Guangdong, China). The signals' integrated optical density (OD) was semi-quantified with ImageJ, using β-actin, GAPDH, tubulin, or Histone 3 as internal references. The primary antibodies used as follows: anti-TH (1:1000; Abcam), anti-LDHA (1:1000, CST), anti-Hexokinase 2 (HK2; 1:1000, Abcam), anti-Interleukin-1β (IL-1β) antibody (1:1000; Abcam), anti-IL-6 (1:1000, CST), anti-inducible nitric oxide synthase (iNOS; 1:1000; Abcam), anti-tumor necrosis factor-α (TNF-α; 1:1000, CST), anti-Arginase 1 (ARG1; 1:1000, CST), anti-NOD-like receptor thermal protein domain associated protein 3 (NLRP3; 1:1000, abclonal), anti-CREB-binding protein C (CREB-BP, CBP; 1:1000, Affinity), anti-p300 (1:1000, Affbiotech), anti-SLC7A11 (1:100, Proteintech), anti-pan-Kla, H3K9la, H3K18la, H3K56la, H4K12la, H4K8la, H4K5la, and H4K16la (1:1000; PTM BIO). Secondary antibody reactions were anti-mouse or anti-rabbit IgG-HRP antibodies (1:5000; Cat#SA00001-2; Proteintech).

Quantitative real-time PCR (qPCR)

Total RNA was isolated from brain tissue or primary microglia using RNAiso Plus reagent (Beijing Tsingke Biology Co., Ltd.). cDNA was synthesized using a PrimeScript RT Reagent Kit (Vazyme). Quantitative real-time PCR (qPCR) was performed on a CFX Connect Real-Time PCR Detection System (Bio-Rad Laboratories, Inc, Hercules, USA) or LightCycler 480II (Roche Diagnostics GmbH, Mannheim, Germany) using the SYBR Green Quantitative RT-PCR Kit (Yeasen Biotechnology Co., Ltd. Shanghai). Relative transcription levels were determined using the $2^{-\Delta\Delta CT}$ method with *Actb* as the reference gene. Primer sequences used in this study are listed in Table. S1.

Table S1. Primer sequences.

Gene name	Species	Primer direction	Primer sequence
Actb	Mouse	Forward primer	GTACTCTGTGTGGATCGGTGG
		Reverse primer	AAAACGCAGCTCAGTAACAGTC
Nos2	Mouse	Forward primer	GTTCTCAGCCCAACAATACAAGA
		Reverse primer	GTGGACGGGTCGATGTCAC
Glut1	Mouse	Forward primer	CCCCGTCCTGCTGCTATTG
		Reverse primer	GCACCGTGAAGATGATGAAGAC
Hk2	Mouse	Forward primer	ATGATCGCCTGCTTATTCACG
		Reverse primer	CGCCTAGAAATCTCCAGAAGGG
Ldha	Mouse	Forward primer	TGTCTCCAGCAAAGACTACTGT
		Reverse primer	GACTGTACTTGACAATGTTGGGA
Nlrp3	Mouse	Forward primer	TGGATGGGTTTGCTGGGAT
		Reverse primer	CTGCGTGTAGCGACTGTTGAG
Il1b	Mouse	Forward primer	TCTTTGAAGTTGACGGACCC
		Reverse primer	TGAGTGATACTGCCTGCCTG
Tnf	Mouse	Forward primer	AGACCCTCACACTCACAAACCAC
		Reverse primer	GCACGTAGTCGGGGCAGC
Il6	Mouse	Forward primer	TAGTCCTTCCTACCCCAATTTCC
		Reverse primer	TTGGTCCTTAGCCACTCCTTC
Mrc1	Mouse	Forward primer	CTCTGTTCAGCTATTGGACGC
		Reverse primer	TGGCACTCCCAAACATAATTTGA
Arg1	Mouse	Forward primer	TTGGGTGGATGCTCACACTG
		Reverse primer	GTACACGATGTCTTTGGCAGA
Ym1	Mouse	Forward primer	CAGGGTAATGAGTGGGTTGG

		Reverse primer	CACGGCACCTCCTAAATTGT
p300	Mouse	Forward primer	GAACAGGAAGAGGAAGAGAGGAAAC
		Reverse primer	TGAGAAAGGTCATTAGACACATTGG
Crebbp	Mouse	Forward primer	GGCCAGGACCGCTTTGTTTATA
		Reverse primer	ATCTTATGGGTGTGGCTCTTTGT
Slc7a11	Mouse	Forward primer	CTTTGTTGCCCTCTCCTGCTTC
		Reverse primer	CAGAGGAGTGTGCTTGTGGACA
Cd80	Mouse	Forward primer	ACCCCCAACATAACTGAGTCT
		Reverse primer	TTCCAACCAAGAGAAGCGAGG
Cd86	Mouse	Forward primer	TGTTTCCGTGGAGACGCAAG
		Reverse primer	TTGAGCCTTTGTAAATGGGCA
Nlrp3	Mouse	Forward primer	TGGATGGGTTTGCTGGGAT
		Reverse primer	CTGCGTGTAGCGACTGTTGAG

RNA-sequencing

RNA was extracted using TRIzol, and its quality was assessed using the NanoDrop and Agilent systems. The mRNA was purified, fragmented, and used for cDNA synthesis. The library was generated using Hieff NGS® DNA Selection Beads and quantified using a Qubit. The library was then sequenced using DNBSEQ-T7 (Wuhan Bioyi Biotechnology Co., Ltd.). Differential gene expression analysis was performed using DESeq2 (v1.30.1) with the following filtering criteria: fold change |log2FoldChange| > 1 and P < 0.05.

Cleavage under targets and tagmentation (CUT&Tag)

The CUT&Tag experiment was performed using the Hyperactive In-Situ ChIP Library Prep Kit for Illumina (pG-Tn5) (TD901, Vazyme, Nanjing, China). Briefly, the primary microglia were collected and bound to Concanavalin A-coated beads. The cells were then resuspended in an antibody buffer and sequentially incubated with primary antibodies against H3K9la and secondary antibodies. The samples were treated with pA/pG-Tn5 transposase. After transposon activation and tagmentation, DNA was isolated, amplified, and purified to create a library. VAHTS DNA Clean Beads (N411, Vazyme, Nanjing, China) were used during the purification steps of the library construction process. The library was quantified using the

VAHTS Library Quantification Kit for Illumina (Vazyme Biotech) and sequenced on an Illumina NovaSeq 150PE.

Chromatin immunoprecipitation assay (ChIP)-qPCR

ChIP analysis was carried out with an anti-H3K9la antibody (PTM Bio, Hangzhou, China) according to the manufacturer's instructions of the ChIP Assay Kit (CST, #9005). Fold enrichment was determined by qPCR and expressed as a percentage of input chromatin (percentage of input). The primer sequences for the *Slc7a11* promoter were 5'-CACTGTGGCAAGCCCTACA TA-3' (forward) and 5'-CAGTGTAGGCAGGTCCCA TC-3' (reverse).

Statistical analysis

Statistical analyses were performed using GraphPad Prism version 8.0.1. Data are presented as mean ± standard error of the mean (SEM). Two-tailed Student's *t*-tests or one-way analysis of variance (ANOVA) followed by Tukey's multiple test was performed to compare data among groups. $P < 0.05$ was considered statistically significant.

Declarations

Ethical Approval

All animal procedures were approved by the institutional animal care and use committee of Tongji Hospital.

Competing interests

The authors declare no conflict of interest.

Authors' contributions

Q.X.Q and X.Z designed and initiated this study. Q.X.Q conducted most of experiments and wrote the draft. J.Y.L A.K., and J.T.L help to conduct the experiments, D.L.W and Y.Q analyzed the data. Z.J.M, Y.J.X and Z.M revised the manuscript.

Funding

Availability of data and materials

The datasets used during the current study are available from the corresponding author on reasonable request.

References

1. KALIA L V, LANG A E. Parkinson's disease [J]. Lancet, 2015, 386(9996): 896–912.

2. Global, regional, and national burden of neurological disorders, 1990–2016: a systematic analysis for the Global Burden of Disease Study 2016 [J]. Lancet Neurol, 2019, 18(5): 459–80.

3. STOKHOLM M G, IRANZO A, ØSTERGAARD K, et al. Assessment of neuroinflammation in patients with idiopathic rapid-eye-movement sleep behaviour disorder: a case-control study [J]. Lancet Neurol, 2017, 16(10): 789–96.

4. HARMS A S, FERREIRA S A, ROMERO-RAMOS M. Periphery and brain, innate and adaptive immunity in Parkinson's disease [J]. Acta Neuropathol, 2021, 141(4): 527–45.

5. LONG-SMITH C M, SULLIVAN A M, NOLAN Y M. The influence of microglia on the pathogenesis of Parkinson's disease [J]. Prog Neurobiol, 2009, 89(3): 277–87.

6. HOLLAND R, MCINTOSH A L, FINUCANE O M, et al. Inflammatory microglia are glycolytic and iron retentive and typify the microglia in APP/PS1 mice [J]. Brain Behav Immun, 2018, 68: 183–96.

7. SMITH A M, DEPP C, RYAN B J, et al. Mitochondrial dysfunction and increased glycolysis in prodromal and early Parkinson's blood cells [J]. Mov Disord, 2018, 33(10): 1580–90.

8. LU J, WANG C, CHENG X, et al. A breakdown in microglial metabolic reprogramming causes internalization dysfunction of α-synuclein in a mouse model of Parkinson's disease [J]. J Neuroinflammation, 2022, 19(1): 113.

9. BAIK S H, KANG S, LEE W, et al. A Breakdown in Metabolic Reprogramming Causes Microglia Dysfunction in Alzheimer's Disease [J]. Cell Metabolism, 2019, 30(3).

10. ANDERSSON A K, RöNNBäCK L, HANSSON E. Lactate induces tumour necrosis factor-alpha, interleukin-6 and interleukin-1beta release in microglial- and astroglial-enriched primary cultures [J]. J Neurochem, 2005, 93(5): 1327–33.

11. SAMUVEL D J, SUNDARARAJ K P, NAREIKA A, et al. Lactate boosts TLR4 signaling and NF-kappaB pathway-mediated gene transcription in macrophages via monocarboxylate transporters and MD-2 up-regulation [J]. J Immunol, 2009, 182(4): 2476–84.

12. LI J, CHEN L, QIN Q, et al. Upregulated hexokinase 2 expression induces the apoptosis of dopaminergic neurons by promoting lactate production in Parkinson's disease [J]. Neurobiology of Disease, 2022, 163: 105605.

13. DISKIN C, RYAN T A J, O'NEILL L A J. Modification of Proteins by Metabolites in Immunity [J]. Immunity, 2021, 54(1): 19–31.

14. ZHANG D, TANG Z, HUANG H, et al. Metabolic regulation of gene expression by histone lactylation [J]. Nature, 2019, 574(7779): 575–80.

15. IRIZARRY-CARO R A, MCDANIEL M M, OVERCAST G R, et al. TLR signaling adapter BCAP regulates inflammatory to reparatory macrophage transition by promoting histone lactylation [J]. Proc Natl Acad Sci U S A, 2020, 117(48): 30628–38.

16. XIONG J, HE J, ZHU J, et al. Lactylation-driven METTL3-mediated RNA mA modification promotes immunosuppression of tumor-infiltrating myeloid cells [J]. Mol Cell, 2022, 82(9).

17. HAGIHARA H, SHOJI H, OTABI H, et al. Protein lactylation induced by neural excitation [J]. Cell Rep, 2021, 37(2): 109820.

18. TANG Y, LE W. Differential Roles of M1 and M2 Microglia in Neurodegenerative Diseases [J]. Mol Neurobiol, 2016, 53(2): 1181–94.

19. PAN R-Y, HE L, ZHANG J, et al. Positive feedback regulation of microglial glucose metabolism by histone H4 lysine 12 lactylation in Alzheimer's disease [J]. Cell Metabolism, 2022, 34(4).

20. DOMERCQ M, SZCZUPAK B, GEJO J, et al. PET Imaging with [(18)F]FSPG Evidences the Role of System xc(-) on Brain Inflammation Following Cerebral Ischemia in Rats [J]. Theranostics, 2016, 6(11): 1753–67.

21. YANG K, FAN M, WANG X, et al. Lactate promotes macrophage HMGB1 lactylation, acetylation, and exosomal release in polymicrobial sepsis [J]. Cell Death Differ, 2022, 29(1): 133–46.

22. QIAO H, HE X, ZHANG Q, et al. Alpha-synuclein induces microglial migration via PKM2-dependent glycolysis [J]. Int J Biol Macromol, 2019, 129: 601–7.

23. ALDANA B I. Microglia-Specific Metabolic Changes in Neurodegeneration [J]. J Mol Biol, 2019, 431(9): 1830–42.

24. LUO G, WANG X, CUI Y, et al. Metabolic reprogramming mediates hippocampal microglial M1 polarization in response to surgical trauma causing perioperative neurocognitive disorders [J]. J Neuroinflammation, 2021, 18(1): 267.

25. LU L, WANG H, LIU X, et al. Pyruvate kinase isoform M2 impairs cognition in systemic lupus erythematosus by promoting microglial synaptic pruning via the β-catenin signaling pathway [J]. J Neuroinflammation, 2021, 18(1): 229.

26. GU R, ZHANG F, CHEN G, et al. Clk1 deficiency promotes neuroinflammation and subsequent dopaminergic cell death through regulation of microglial metabolic reprogramming [J]. Brain Behav Immun, 2017, 60: 206–19.

27. YE L, JIANG Y, ZHANG M. Crosstalk between glucose metabolism, lactate production and immune response modulation [J]. Cytokine Growth Factor Rev, 2022.

28. LI X, YANG Y, ZHANG B, et al. Lactate metabolism in human health and disease [J]. Signal Transduct Target Ther, 2022, 7(1): 305.

29. PUCINO V, CERTO M, BULUSU V, et al. Lactate Buildup at the Site of Chronic Inflammation Promotes Disease by Inducing CD4 T Cell Metabolic Rewiring [J]. Cell Metabolism, 2019, 30(6).

30. KAUSHIK D K, BHATTACHARYA A, MIRZAEI R, et al. Enhanced glycolytic metabolism supports transmigration of brain-infiltrating macrophages in multiple sclerosis [J]. J Clin Invest, 2019, 129(8): 3277–92.

31. SCHIRINZI T, DI LAZZARO G, SANCESARIO G M, et al. Young-onset and late-onset Parkinson's disease exhibit a different profile of fluid biomarkers and clinical features [J]. Neurobiol Aging, 2020,

90: 119–24.

32. DAI S-K, LIU P-P, LI X, et al. Dynamic profiling and functional interpretation of histone lysine crotonylation and lactylation during neural development [J]. Development, 2022, 149(14).

33. SATO H, TAMBA M, ISHII T, et al. Cloning and expression of a plasma membrane cystine/glutamate exchange transporter composed of two distinct proteins [J]. J Biol Chem, 1999, 274(17): 11455–8.

34. DOS-SANTOS-PEREIRA M, ACUñA L, HAMADAT S, et al. Microglial glutamate release evoked by α-synuclein aggregates is prevented by dopamine [J]. Glia, 2018, 66(11): 2353–65.

35. MESCI P, ZAïDI S, LOBSIGER C S, et al. System xC- is a mediator of microglial function and its deletion slows symptoms in amyotrophic lateral sclerosis mice [J]. Brain, 2015, 138(Pt 1): 53–68.

36. SPRIMONT L, JANSSEN P, DE SWERT K, et al. Cystine-glutamate antiporter deletion accelerates motor recovery and improves histological outcomes following spinal cord injury in mice [J]. Sci Rep, 2021, 11(1): 12227.

37. ZUO Y, XIE J, LI X, et al. Ferritinophagy-Mediated Ferroptosis Involved in Paraquat-Induced Neurotoxicity of Dopaminergic Neurons: Implication for Neurotoxicity in PD [J]. Oxid Med Cell Longev, 2021, 2021: 9961628.

38. MATSUSHITA M, FREIGANG S, SCHNEIDER C, et al. T cell lipid peroxidation induces ferroptosis and prevents immunity to infection [J]. J Exp Med, 2015, 212(4): 555–68.

39. KAPRALOV A A, YANG Q, DAR H H, et al. Redox lipid reprogramming commands susceptibility of macrophages and microglia to ferroptotic death [J]. Nat Chem Biol, 2020, 16(3): 278–90.

40. MASCHALIDI S, MEHROTRA P, KEçELI B N, et al. Targeting SLC7A11 improves efferocytosis by dendritic cells and wound healing in diabetes [J]. Nature, 2022, 606(7915): 776–84.

41. QU W, CHENG Y, PENG W, et al. Targeting iNOS Alleviates Early Brain Injury After Experimental Subarachnoid Hemorrhage via Promoting Ferroptosis of M1 Microglia and Reducing Neuroinflammation [J]. Mol Neurobiol, 2022, 59(5): 3124–39.

42. MORENO-YRUELA C, ZHANG D, WEI W, et al. Class I histone deacetylases (HDAC1-3) are histone lysine delactylases [J]. Sci Adv, 2022, 8(3): eabi6696.

43. CUI H, XIE N, BANERJEE S, et al. Lung Myofibroblasts Promote Macrophage Profibrotic Activity through Lactate-induced Histone Lactylation [J]. Am J Respir Cell Mol Biol, 2021, 64(1): 115–25.
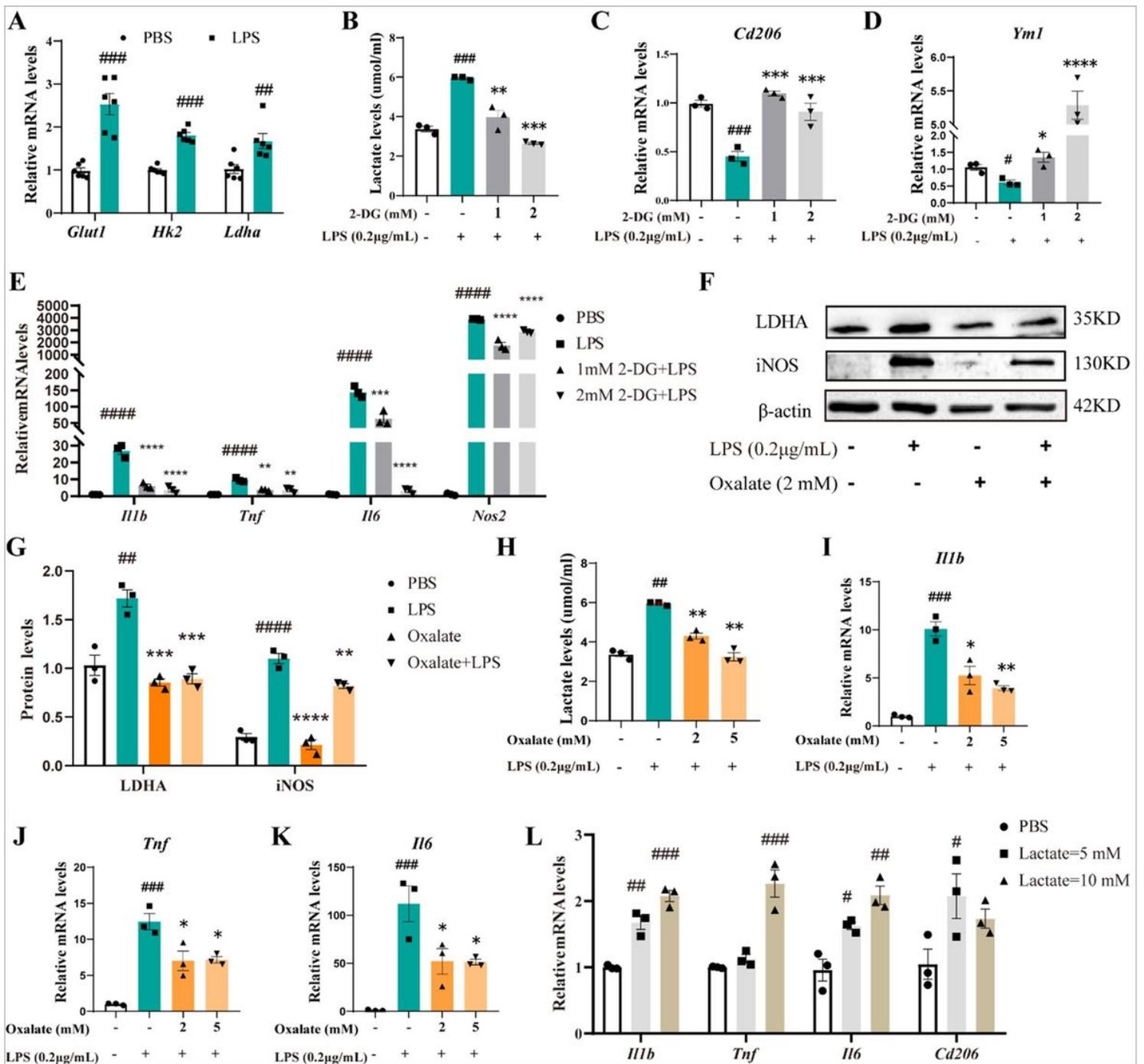
Figures
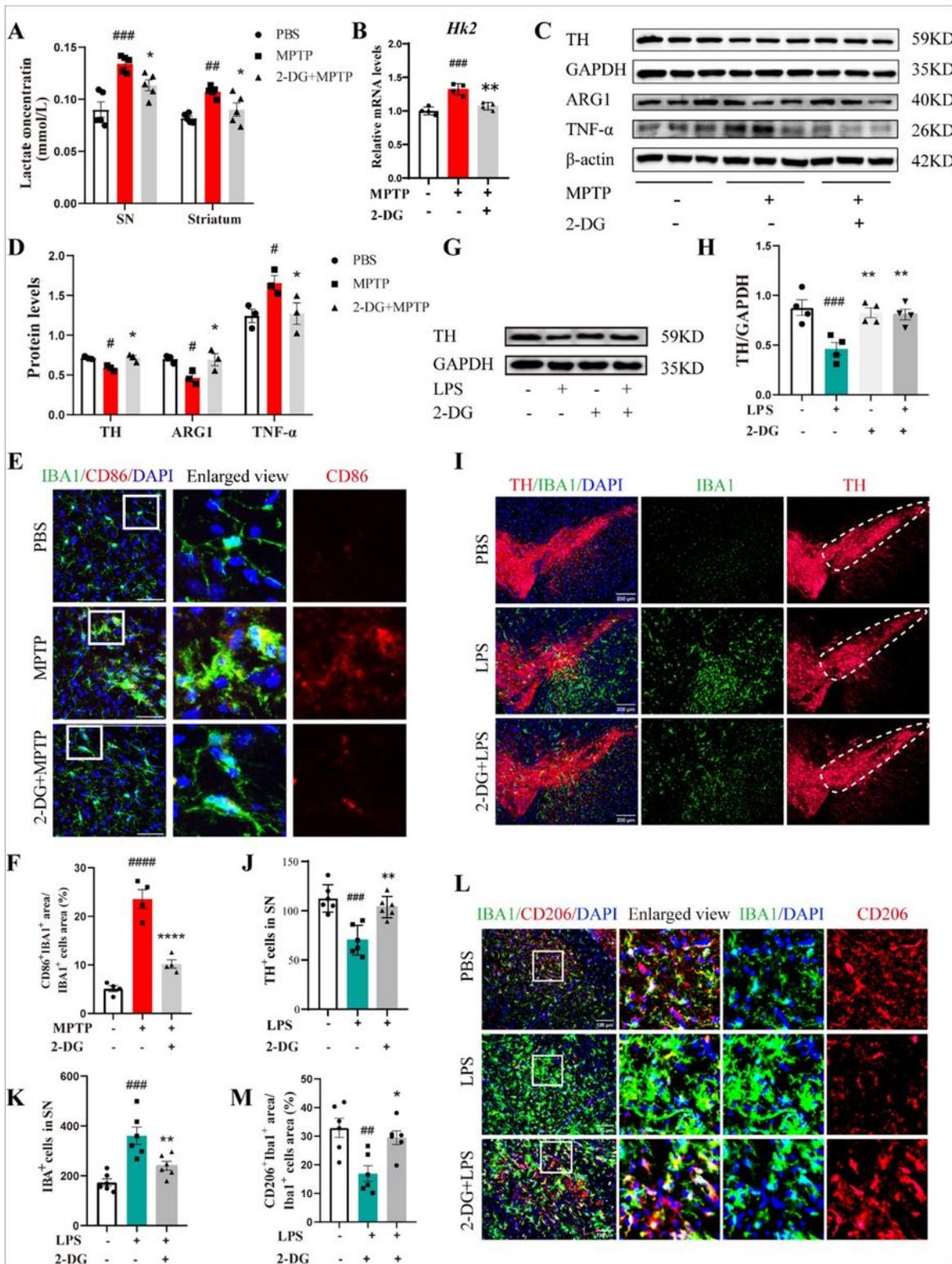
Figure 1

Inhibition of glycolysis improves motor function and alleviates microglial activation in MPTP-induced mouse model of PD. (A) Lactate concentration in the SN and striatum of Control, MPTP, and 2-DG MPTP mice. N=5 per group. (B) Hk2 mRNA expression in the SN of Control, MPTP, and 2-DG-MPTP mice. N=4 per group. (C-D) Representative western blot and quantification of TH, ARG1, and TNF-α in the SN of Control, MPTP, and 2-DG-MPTP mice. N=3~4 per group. (E) Representative confocal images of IBA1

(green) and CD86 (red) in the SN of Control, MPTP, and 2-DG-MPTP mice. Scale bar, 50μm. (F) Quantification of the ratio of CD86$^+$ IBA1$^+$ area to IBA1$^+$ cells area. N=4 per group. (G) Representative western blot and quantification of TH in the SN of Control, LPS, and 2-DG-LPS mice. N=4 per group. (I) Representative images of TH (red) and IBA1 (green) in the SN of Control, LPS, and 2-DG-LPS mice. Scale bar, 200μm. (J-K) Quantification of TH$^+$ cells and IBA1$^+$ cells. N=6 per group. (L) Representative images of IBA1 (green) and CD206 (red) in the SN of Control, LPS, and 2-DG-LPS mice. Scale bar, 100μm. (M) Quantification of the ratio of CD206$^+$IBA1$^+$ area to IBA1$^+$ cells area. N=6~8 per group. Data are shown as the mean ± SEM and analyzed with one-way ANOVA followed by Tukey's multiple comparisons test. Compared to PBS group, $^\#P < 0.05$, $^{\#\#}P < 0.01$, $^{\#\#\#}P < 0.001$, $^{\#\#\#\#}P < 0.0001$; compared to MPTP group or LPS group, $^*P < 0.05$, $^{**}P < 0.01$, $^{***}P < 0.001$.

Figure 2

Enhanced glycolysis-derived lactate promotes microglial activation. Primary microglia pretreated with or without 2-DG for 30 min then stimulate with 0.2 µg/mL LPS for 24h. (A) mRNA expression of Glut1, Hk2 and Ldha. N=6 per group. (B) Lactate concentration. N=3 per group. (C-E) mRNA expression of Cd206, Ym1, Il1b, Tnf, Il6 and Nos2. N=3 per group. Primary microglia pretreated with or without sodium oxalate for 30 min then stimulate with 0.2 µg/mL LPS for 24h. (F-G) Representative western blot and quantification of iNOS and LDHA. N=3 per group. (H-K) Lactate concentration and Il1b, Tnf and Il6 mRNA expression. N=3 per group. (L) mRNA expression of Il1b, Tnf, Il6 and Cd206 mRNA expression in primary microglia stimulated with or without sodium lactate. N=3 per group. Data are shown as the mean ± SEM

and analyzed with one-way ANOVA followed by Tukey's multiple comparisons test. Compared to PBS group, #$P < 0.05$, ##$P < 0.01$, ###$P < 0.001$, ####$P < 0.0001$; compared to LPS group, *$P < 0.05$, **$P < 0.01$, ***$P < 0.001$, ****$P < 0.0001$.
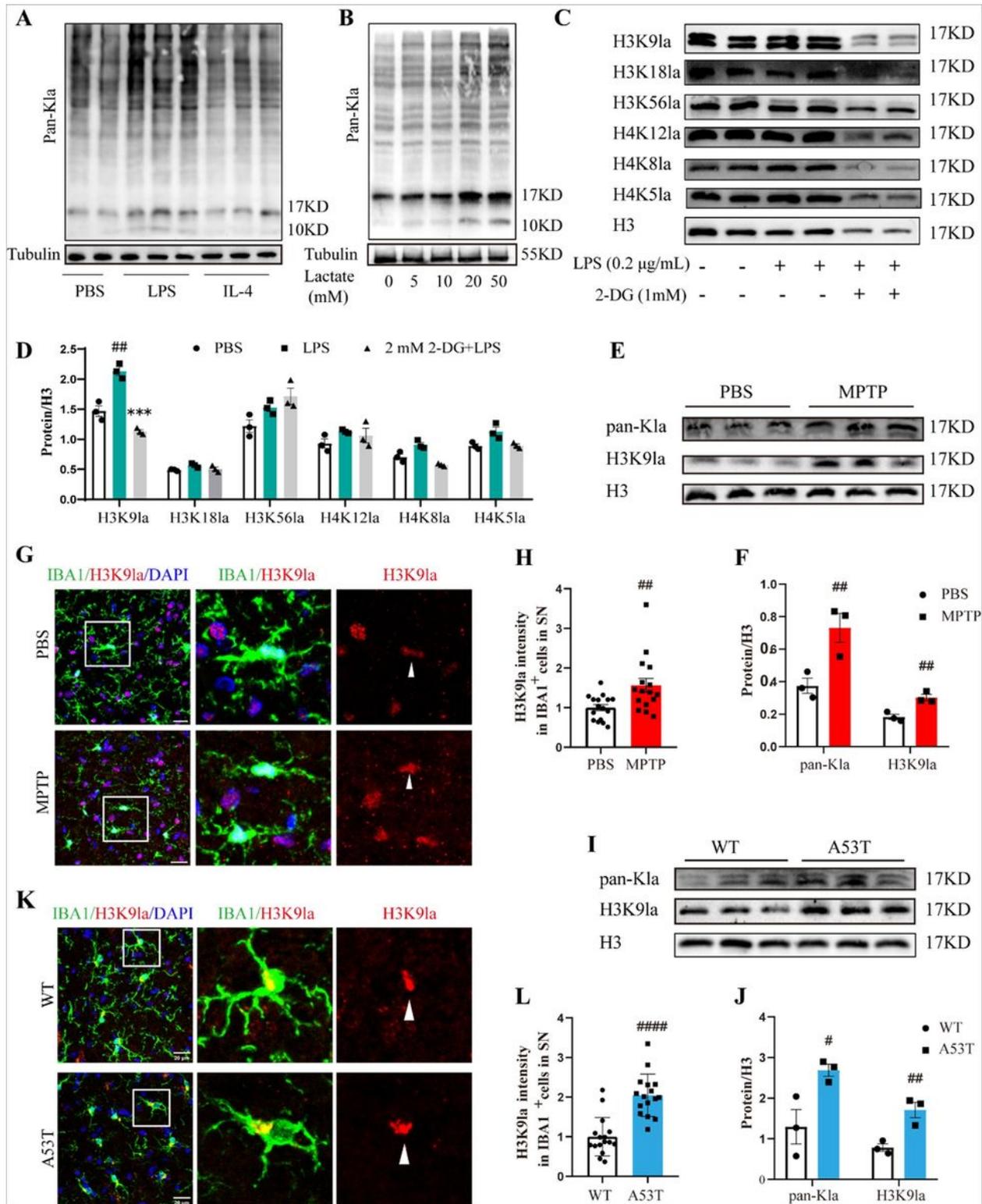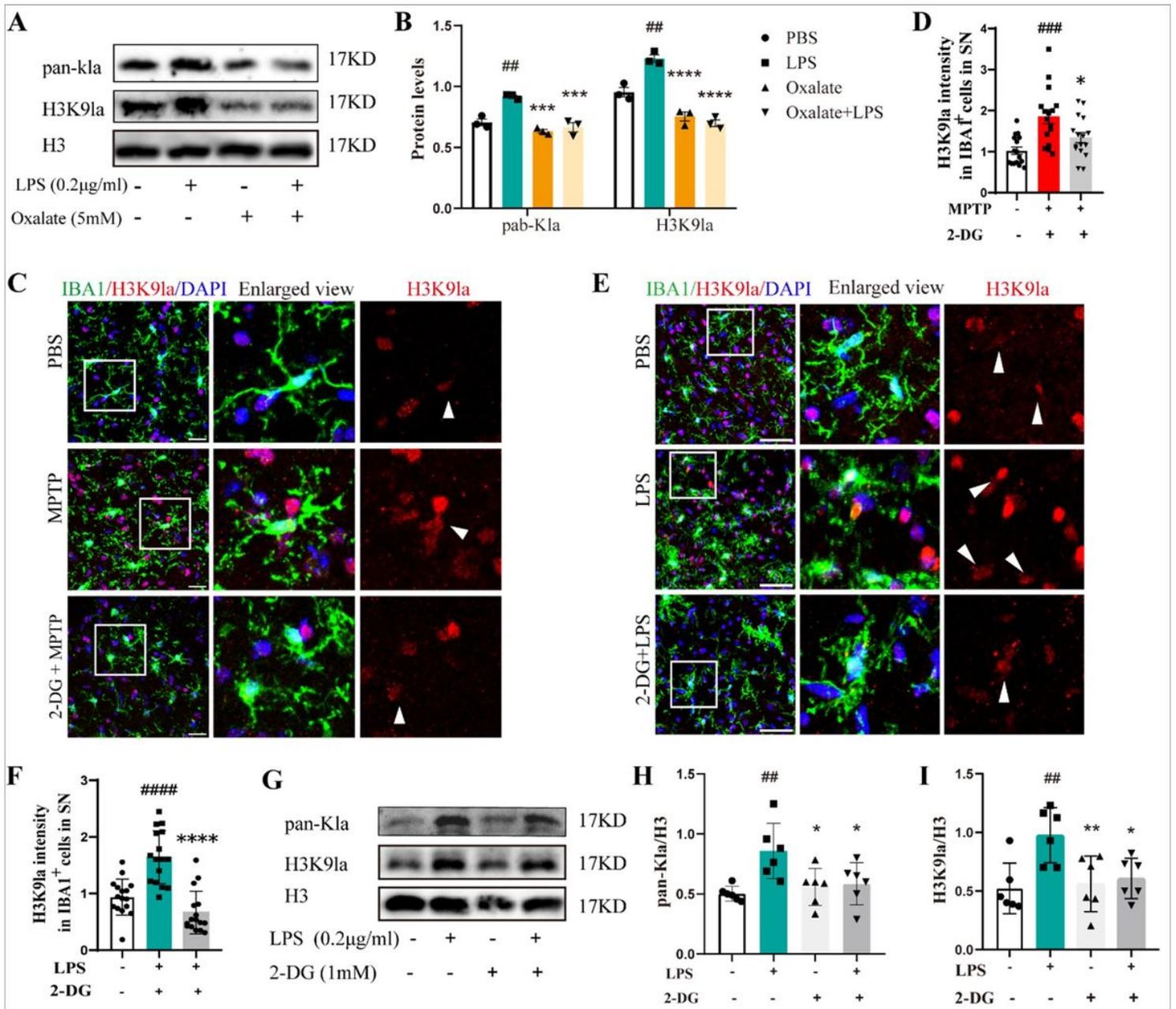

Figure 3

Enhanced glycolysis-derived lactate promotes microglial activation through histone lactylation. (A-B) Representative western blot of pan-Kla in primary microglia treated with PBS and LPS and IL-4 and exogenous lactate. N=1~3 per group. (C-D) Representative western blot and quantification of H3K9la, H3K18la, H3K56la, H4K12la, H4K8la and H4K5la in LPS-stimulated primary microglia treated with or without 2-DG. N=3 per group. (E-F) Representative western blot and quantification of pan-Kla and H3K9la in the SN of Control and MPTP-treated mice. N=3 per group. (G) Representative confocal images of IBA1 (green) and H3K9la (red) in microglia in the SN of Control and MPTP-treated mice. Scale bar, 50 μm. (H) Quantification of fluorescence intensity of H3K9la in microglia in the SN of Control and MPTP mice. N=4 per group. (I-J) Representative western blot and quantification of pan-Kla and H3K9la in the SN of Control and A53T mice. N=3 per group. (K) Representative confocal images of IBA1 (green) and H3K9la (red) in microglia in the SN of Control and A53T mice. Scale bar, 50 μm. (L) Quantification of fluorescence intensity of H3K9la in microglia in the SN of Control and A53T mice. N=4 per group. For fluorescence intensity of H3K9la, four different layers of brain slices were taken from each brain for staining. Two brain slices were 120μm apart, and 4~6 visual fields were taken from each brain slice to average, so there were 4 points in each brain. Data are shown as the mean ± SEM and analyzed with two-tailed unpaired Student's t-test or one-way ANOVA followed by Tukey's multiple comparisons test. Compared to PBS group, $^{\#}P < 0.05$, $^{\#\#}P < 0.01$, $^{\#\#\#}P < 0.001$, $^{\#\#\#\#}P < 0.0001$; compared to LPS group, $^{*}P < 0.05$, $^{**}P < 0.01$, $^{***}P < 0.001$, $^{****}P < 0.0001$.
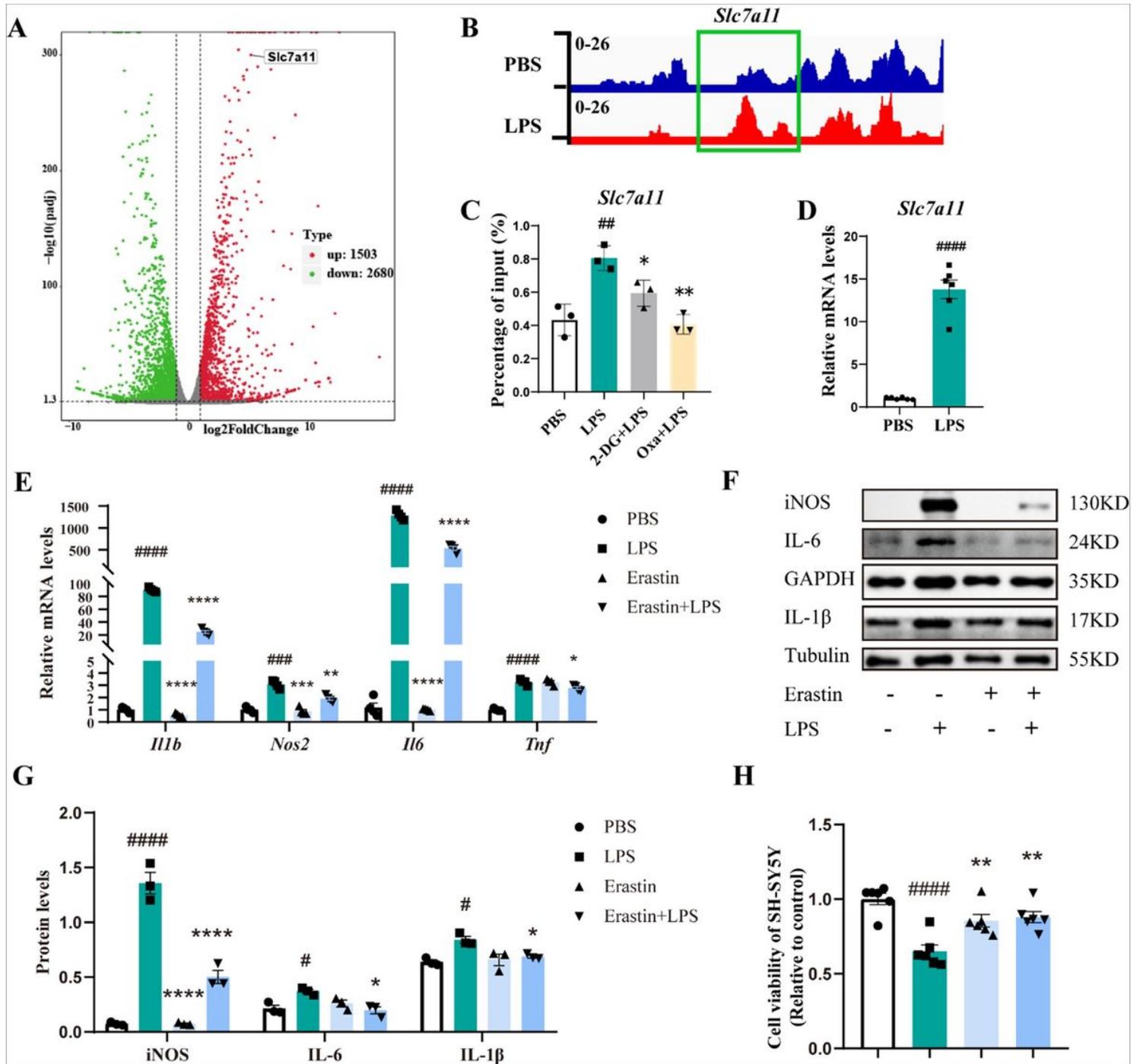
Figure 4

Inhibition of glycolysis reduces the activation of microglia by reducing histone lactylation. (A-B) Representative western blot and quantification of pan-Kla and H3K9la in LPS-stimulated primary microglia treated with or without sodium oxalate. N=3 per group. (C) Representative images of IBA1 (green) and H3K9la (red) in microglia in the SN of Control, MPTP and 2-DG+MPTP mice. Scale bar, 50 μm. (D) Quantification of fluorescence intensity of HK9la in microglia in the SN of Control, MPTP and 2-DG+MPTP mice. N=4 per group. (E) Representative images of IBA1 (green) and H3K9la (red) in microglia in the SN of Control, LPS and 2-DG+LPS mice. Scale bar, 50 μm. (F) Quantification of fluorescence intensity of HK9la in microglia in the SN of Control, LPS and 2-DG+LPS mic. N=4 per group. (G-I) Representative western blot and quantification of pan-Kla and H3K9la in the SN of Control, LPS and 2-DG+LPS mice. N=6 per group. For fluorescence intensity of H3K9la, four different layers of brain slices

were taken from each brain for staining. Two brain slices were 120μm apart, and 4~6 visual fields were taken from each brain slice to average, so there were 4 points in each brain. Data are shown as the mean ± SEM and analyzed with one-way ANOVA followed by Tukey's multiple comparisons test. Compared to PBS group, $^{\#}P < 0.05$, $^{\#\#}P < 0.01$, $^{\#\#\#}P < 0.001$, $^{\#\#\#\#}P < 0.0001$; compared to MPTP group or LPS group, $^{*}P < 0.05$, $^{**}P < 0.01$, $^{***}P < 0.001$, $^{****}P < 0.0001$.

Figure 5

Slc7a11 is the target of H3K9la and SLC7A11 inhibition alleviates microglial activation. (A) Volcano plots showing the differentially expressed genes in primary microglia stimulated with or without LPS. N=3 per

group. (B) Genome browser tracks of CUT&Tag signal at the representative target gene loci. The green rectangles indicate the peak regions of H3K9la on Slc7a11 promoters. (C) ChIP-qPCR was performed on LPS-stimulated primary microglia treated with 2-DG or sodium oxalate using anti-H3K9la antibody. N=3 per group. (D) Slc7a11 mRNA expression in primary microglia stimulated with or without LPS. N=6 per group. (E) Il1b, Nos2, Il6, and Tnf mRNA expression in LPS-stimulated primary microglia pretreated with or or without erastin. N=4 per group. (F-G) Representative western blot and quantification of iNOS, IL-6 and IL-1β. N=3 per group. (H) The survival rate of SH-SY5Y cells was assessed by CCK8 assay. N=6 per group. Data are shown as the mean ± SEM and analyzed with two-tailed unpaired Student's t-test or one-way ANOVA followed by Tukey's multiple comparisons test. Compared to PBS group, $^{#}P < 0.05$, $^{##}P < 0.01$, $^{###}P < 0.001$, $^{####}P < 0.0001$; compared to LPS group, $^{*}P < 0.05$, $^{**}P < 0.01$, $^{***}P < 0.001$, $^{****}P < 0.0001$.
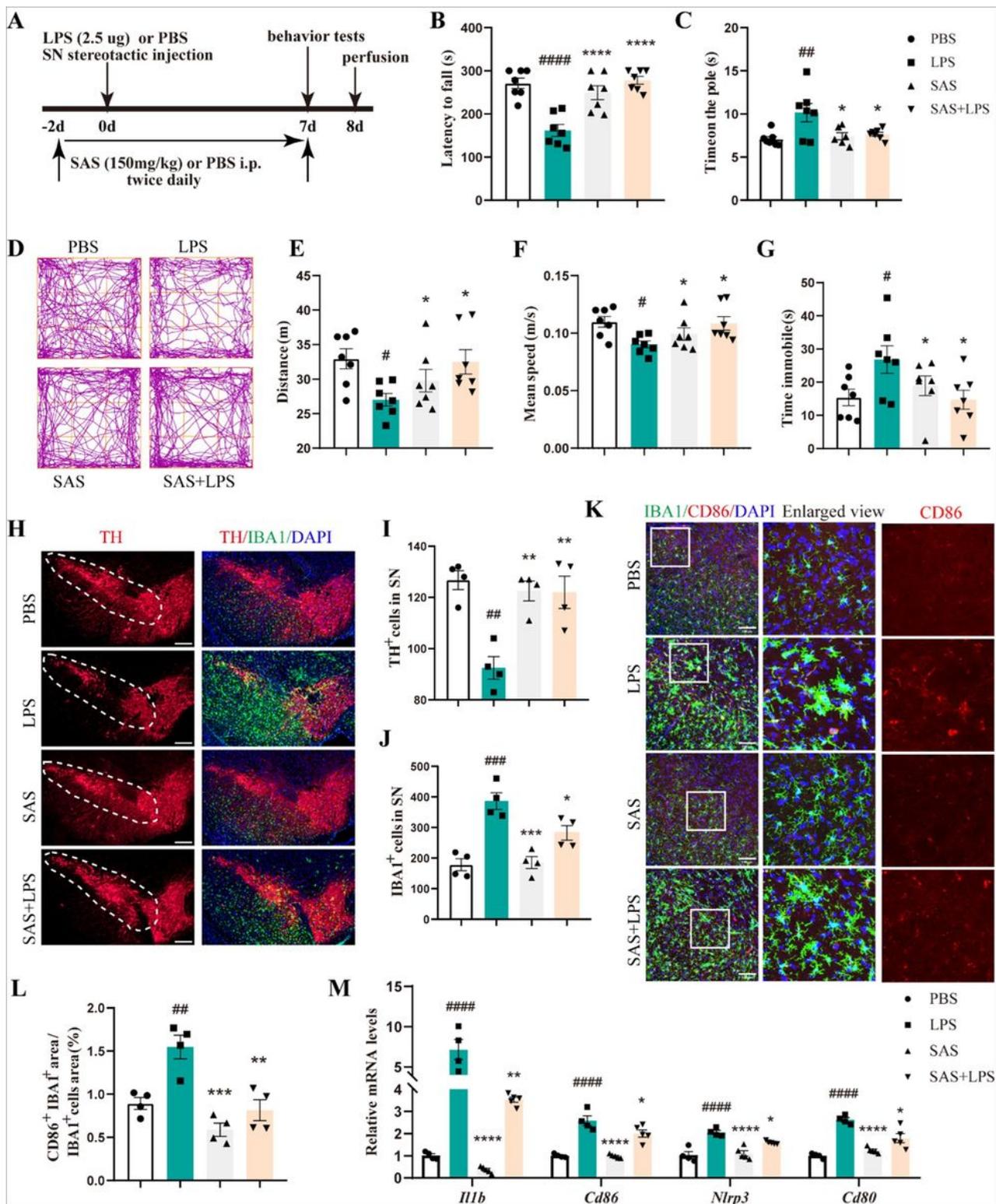
Figure 6

Inhibition of SLC7A11 improves motor dysfunction and attenuates microglial activation in LPS induced-PD mice. (A) Experimental schedule. (B-C) Quantification of latency to fall in rotarod test, time on the pole in pole test of Control, LPS, SAS, and SAS+LPS mice. N=7 per group. (D) Representative track of mouse movement in OFT. (E-G) Quantification of total distance, mean speed, and immobility time in OFT. N=7 per group. (H) (L) Representative images staining of IBA1 (green) and TH (red) in the SN of Control, LPS,

SAS and SAS LPS mice. Scale bar, 200μm. (I-J) Quantification of TH⁺ cells and IBA1⁺ cells. N=4 per group. (K) Representative images staining of IBA1 (green) and CD86 (red) in the SN of Control, LPS, SAS and SAS LPS mice. Scale bar, 100μm. (L) Quantification of the ratio of CD86⁺IBA1⁺ area to IBA1⁺ cells area. N=4 per group. (M) Il1b, Cd86, Nlrp3 and Cd80 mRNA expression in the SN of Control, LPS, SAS and SAS+LPS mice. N=4 per group. Data are shown as the mean ± SEM and analyzed with one-way ANOVA followed by Tukey's multiple comparisons test. Compared to PBS group, $^{\#}P < 0.05$, $^{\#\#}P < 0.01$, $^{\#\#\#}P < 0.001$, $^{\#\#\#\#}P < 0.0001$; compared to LPS group, $^{*}P < 0.05$, $^{**}P < 0.01$, $^{***}P < 0.001$, $^{****}P < 0.0001$.
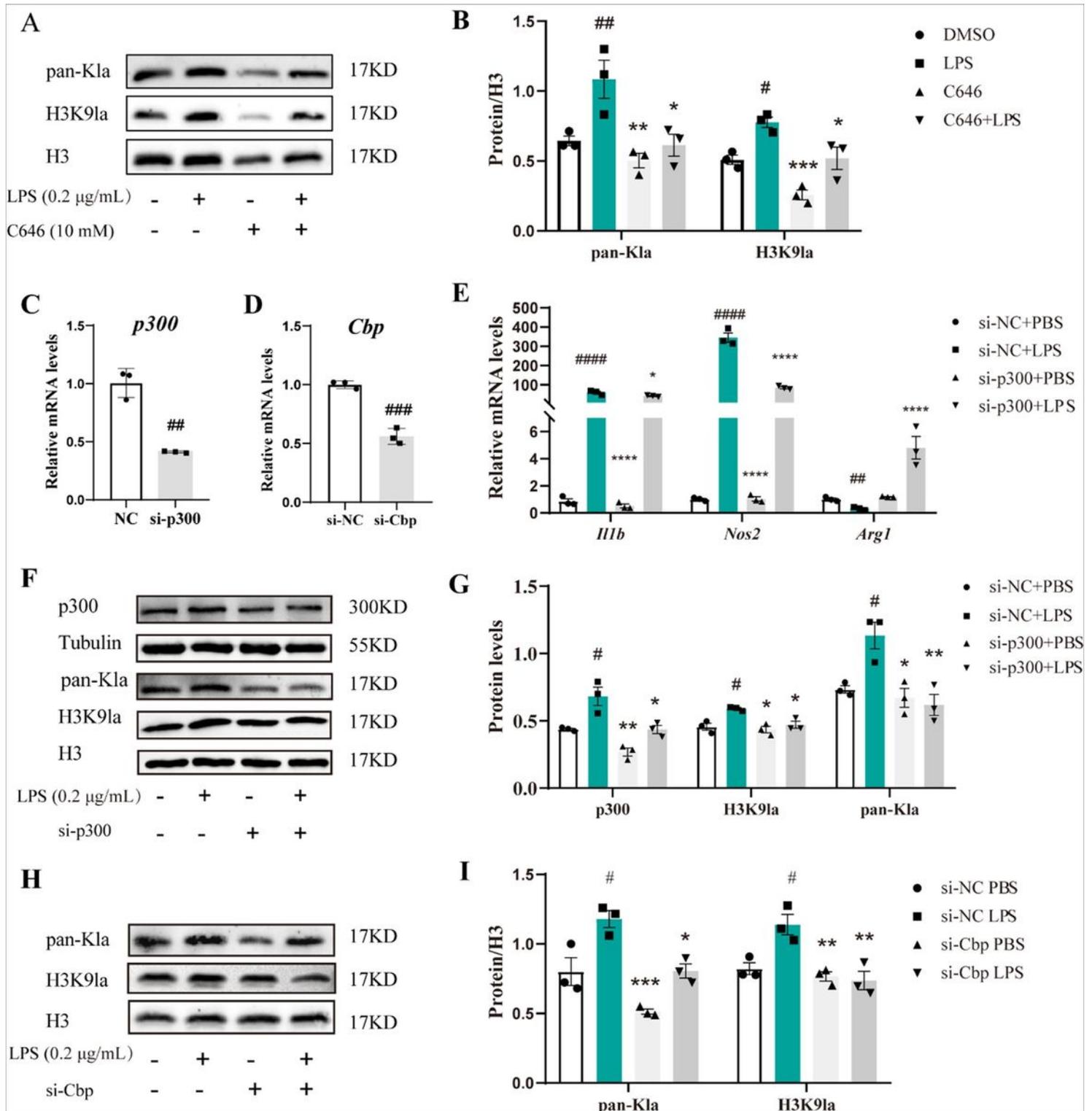
Figure 7

p300/CBP mediates pan-Kla and H3K9la in LPS-stimulated primary microglia. (A-B) Representative western blot and quantification of pan-Kla and H3K9la in LPS-stimulated primary microglia treated with or without C646. N=3 per group. (C-D) p300 and Cbp mRNA expression in primary microglia transfected with si-p300 or si-Cbp. N=3 per group. (E) Il1b, Nos2, and Arg1 mRNA expression in primary microglia transfected with si-p300 and stimulated with or without LPS. N=3 per group. (F-G) Representative western blot and quantification of p300, pan-Kla and H3K9la in primary microglia transfected with si-p300 and stimulated with or without LPS. N=3 per group. (H-I) Representative western blot and quantification of pan-Kla and H3K9la in primary microglia transfected with si-Cbp and stimulated with or without LPS. N=3 per group. Data are shown as the mean ± SEM and analyzed with two-tailed unpaired Student's t-test or one-way ANOVA followed by Tukey's multiple comparisons test. Compared to PBS group, $^{\#}P < 0.05$, $^{\#\#}P < 0.01$, $^{\#\#\#}P < 0.001$, $^{\#\#\#\#}P < 0.0001$; compared to LPS group, $^{*}P < 0.05$, $^{**}P < 0.01$, $^{***}P < 0.001$, $^{****}P < 0.0001$.

Supplementary Files

This is a list of supplementary files associated with this preprint. Click to download.

- floatimage1.jpg
- WB.docx
- SupplementaryMaterial.docx